Engineering Structures 69 (2014) 83–89

Contents lists available at ScienceDirect

Engineering Structures

journal homepage: www.elsevier.com/locate/engstruct

A direct method for analyzing the nonlinear vehicle–structure interaction

S.G.M. Neves [a,b,*], P.A. Montenegro [b], A.F.M. Azevedo [b], R. Calçada [b]

[a] ISEP, Polytechnic Institute of Porto, Rua Dr. António Bernardino de Almeida, 431, 4200-072 Porto, Portugal
[b] Centro de Estudos da Construção, Faculdade de Engenharia, Universidade do Porto, Rua Dr. Roberto Frias, 4200-465 Porto, Portugal

ARTICLE INFO

Article history:
Received 28 September 2013
Revised 24 February 2014
Accepted 25 February 2014
Available online 5 April 2014

Keywords:
Vehicle–structure interaction
Nonlinear contact
Contact element
Dynamic analysis

ABSTRACT

This article presents an accurate, efficient and stable algorithm to analyze the nonlinear vertical vehicle–structure interaction. The governing equilibrium equations of the vehicle and structure are complemented with additional constraint equations that relate the displacements of the vehicle with the corresponding displacements of the structure. These equations form a single system, with displacements and contact forces as unknowns, that is solved using an optimized block factorization algorithm. Due to the nonlinear nature of contact, an incremental formulation based on the Newton method is adopted. The vehicles, track and structure are modeled using finite elements to take into account all the significant deformations. The numerical example presented clearly demonstrates the accuracy and computational efficiency of the proposed method.

1. Introduction

The development of efficient and robust algorithms that can accurately analyze the nonlinear vehicle-structure interaction is still an important issue, especially due to the increase of the corresponding operating speeds.

A vehicle-structure interaction problem is considerably more complex than a typical structural dynamics problem due to the relative movement between the two subsystems and the associated constraint equations relating the vehicle and structure displacements. In a significant number of studies available in the literature about the vehicle–structure interaction, the structure and vehicles are modeled as rigid multibody systems [1,2]. Other authors, such as Antolín et al. [3] and Tanabe et al. [4], proposed formulations that additionally take into account the deformation of the structure. Neves et al. [5] modeled the vehicles and structure using finite elements, thus considering the deformation of both systems.

When the vehicle and structure are considered as a single system, the forces acting on the contact interface are internal forces. Since the vehicle moves relatively to the structure, to avoid calculating and assembling the element matrices at each time step Yang and Wu [6] proposed a new contact element based on a condensation technique that eliminates the degrees of freedom at the contact interface. However, since the matrices of these elements depend on the position of the contact points, the global stiffness matrix is time-dependent and must be updated and factorized at each time step. This procedure may demand a considerable computational effort.

When the vehicle and structure are treated as separate systems, two different approaches can be adopted: variational formulations that consider an additional term in the energy of the system can be used to impose the constraints [7], or the contact forces can be considered explicitly and treated as externally applied loads, being the equilibrium of all forces acting on the contact interface established directly.

In the methods described in [8–11] the contact forces are considered explicitly but are not treated as unknowns of the governing equilibrium equations. An iterative procedure is used to ensure the coupling between the two subsystems. These methods may exhibit a slow rate of convergence, especially when unilateral contact is considered or a large number of contact points are required. To overcome these limitations, Neves et al. [5] developed an accurate, efficient and robust algorithm to analyze the vertical vehicle–structure interaction, referred to as the direct method, in which the governing equilibrium equations of the vehicle and structure are complemented with additional constraint equations that relate the displacements of the contact nodes of the vehicle with the corresponding nodal displacements of the structure, with no

* Corresponding author at: ISEP, Polytechnic Institute of Porto, Rua Dr. António Bernardino de Almeida, 431, 4200-072 Porto, Portugal. Tel.: +351 22 508 1901; fax: +351 22 508 1446.

E-mail addresses: sgm.neves@fe.up.pt (S.G.M. Neves), pedro.montenegro@fe.up.pt (P.A. Montenegro), alvaro@fe.up.pt (A.F.M. Azevedo), ruiabc@fe.up.pt (R. Calçada).

http://dx.doi.org/10.1016/j.engstruct.2014.02.027
0141-0296/

separation being allowed. These equations form a single system, with displacements and contact forces as unknowns, that is solved directly using an optimized block factorization algorithm. The Lagrange multiplier method and the direct method are equivalent and lead to identical systems of linear equations. The main advantage of the direct equilibrium of forces, when compared with the variational formulations, is a better understanding of the physical meaning of the contact forces, which is particularly important in complex problems such as the vehicle–structure interaction.

In the present article a search algorithm is used to detect which elements are in contact, being the constraints imposed when contact occurs. The time integration is performed using the α method since it provides numerical dissipation in the higher modes while maintaining second-order accuracy [12]. The proposed methodology is implemented in MATLAB [13]. The vehicles and structure are modeled with ANSYS [14], being their structural matrices imported by MATLAB.

2. Contact and target elements

When studying the contact between two bodies, one conventionally has a contact surface, and the other a target surface (see Fig. 1). A two-dimensional node-to-segment contact element is used in the present formulation.

The direct method [5] introduces additional variables in the system to impose the contact conditions, whereas in the penalty method no additional variables are required. Increasing values of the penalty parameter lead to more accurate solutions, but the coefficient matrix might become ill-conditioned. In railway engineering the number of contact points is usually small when compared with the total size of the problem. For this reason, the use of the direct method leads to a small additional computational cost but has the advantage of avoiding ill-conditioned systems.

In the formulation proposed in [5] the contact constraint equations are imposed using the direct method, with no separation being allowed. In the present formulation a search algorithm is used to detect which elements are in contact, being the constraints imposed when contact occurs. Since in the present formulation only the frictionless contact is considered, the constraint equations are purely geometrical and relate the displacements of the contact node with the displacements of the corresponding target element.

Fig. 2 shows the two-dimensional node-to-segment contact element implemented in the present formulation and the local coordinate system (ξ_1, ξ_2, ξ_3) of the contact pair. The ξ_2 axis always points towards the contact node, being the two elements separated by an initial gap g. The forces acting at the contact interface are denoted by X and the superscripts CE and TE indicate contact and target elements, respectively.

According to Newton's third law, the forces acting at the contact interface must be of equal magnitude and opposite direction, i.e.,

$$\mathbf{X}^{CE} + \mathbf{X}^{TE} = \mathbf{0} \tag{1}$$

The displacement vector of an arbitrary point is defined by two translations, v_{ξ_1} and v_{ξ_2}, and a rotation θ_{ξ_3} about the ξ_3 axis. Since this type of contact element neglects the tangential forces and moments transmitted across the contact interface, the contact constraint equations only relate the displacement v_{ξ_2} of the contact node with the corresponding displacement of the auxiliary point k. Each constraint equation is defined in the local coordinate system of the contact pair and comprises the non-penetration condition for the normal direction. These equations are given by

$$\mathbf{v}^{CE} - \mathbf{v}^{TE} \geq -\mathbf{g} + \mathbf{r} \tag{2}$$

where $\mathbf{r}$ are the irregularities between the contact and target elements. The gaps are always positive and a positive irregularity implies an increase of the distance between the contact and target elements (see Fig. 2).

3. Equations of motion

3.1. Force equilibrium

The α method is an implicit time integration scheme that is generally accurate and stable [12]. Assuming that the applied loads are deformation-independent and that the nodal point forces corresponding to the internal element stresses may depend nonlinearly on the nodal point displacements, the equations of motion of the vehicle–structure system given in [5] may be rewritten in the form

$$\begin{aligned}&\mathbf{M}\mathbf{a}^{t+\Delta t} + \mathbf{C}[(1+\alpha)\dot{\mathbf{a}}^{t+\Delta t} - \alpha\dot{\mathbf{a}}^{t}] + (1+\alpha)\mathbf{R}^{t+\Delta t} - \alpha\mathbf{R}^{t}\\ &\quad = (1+\alpha)\mathbf{F}^{t+\Delta t} - \alpha\mathbf{F}^{t}\end{aligned} \tag{3}$$

where $\mathbf{M}$ is the mass matrix, $\mathbf{C}$ is the viscous damping matrix, $\mathbf{R}$ are the nodal forces corresponding to the internal element stresses, $\mathbf{F}$ are the externally applied nodal loads and $\mathbf{a}$ are the nodal displacements. The superscripts t and $t+\Delta t$ indicate the previous and current time steps, respectively.

To solve Eq. (3) let the F type degrees of freedom (d.o.f.) represent the free nodal d.o.f., whose values are unknown, and let the P type d.o.f. represent the prescribed nodal d.o.f., whose values are known. Thus, the load vector can be expressed as

$$\mathbf{F}_F = \mathbf{P}_F + \mathbf{D}_{FX}^{CE}\mathbf{X}^{CE} + \mathbf{D}_{FX}^{TE}\mathbf{X}^{TE} \tag{4}$$

$$\mathbf{F}_P = \mathbf{P}_P + \mathbf{D}_{PX}^{CE}\mathbf{X}^{CE} + \mathbf{D}_{PX}^{TE}\mathbf{X}^{TE} + \mathbf{S} \tag{5}$$

where $\mathbf{P}$ corresponds to the externally applied nodal loads whose values are known and $\mathbf{S}$ are the support reactions, whose values are unknown. Each matrix $\mathbf{D}$ relates the contact forces, defined in the local coordinate system of the respective contact pair, with the nodal forces defined in the global coordinate system (see Fig. 2).

Substituting Eq. (1) into Eqs. (4) and (5) leads to

$$\mathbf{F}_F = \mathbf{P}_F + \mathbf{D}_{FX}\mathbf{X} \tag{6}$$

$$\mathbf{F}_P = \mathbf{P}_P + \mathbf{D}_{PX}\mathbf{X} + \mathbf{S} \tag{7}$$

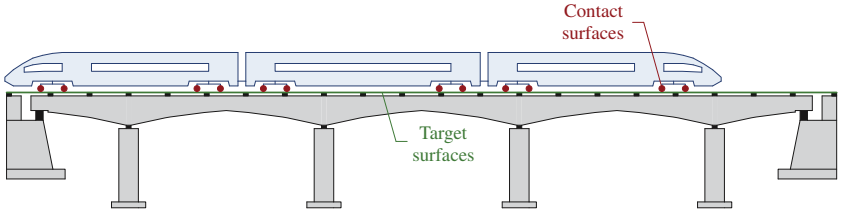

Fig. 1. Contact pair concept.

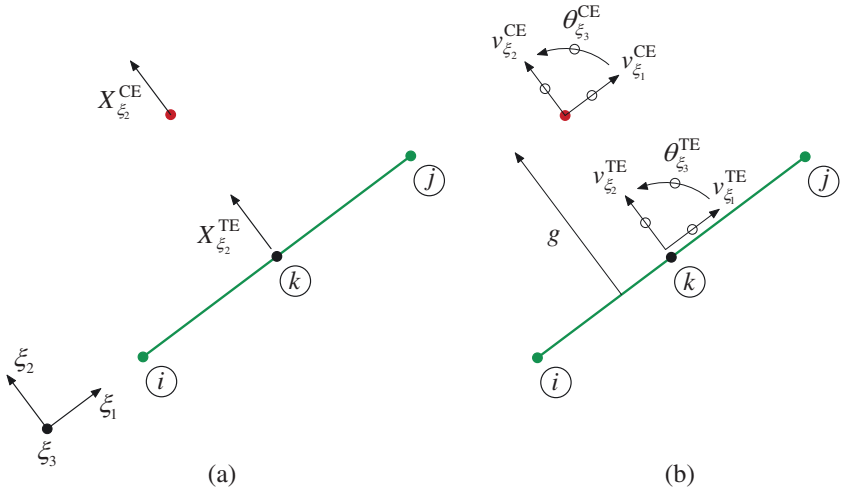

Fig. 2. Node-to-segment contact element: (a) forces and (b) displacements at the contact interface.

where

$$\mathbf{X} = \mathbf{X}^{CE} \tag{8}$$

$$\mathbf{D}_{FX} = \mathbf{D}^{CE}_{FX} - \mathbf{D}^{TE}_{FX} \tag{9}$$

$$\mathbf{D}_{PX} = \mathbf{D}^{CE}_{PX} - \mathbf{D}^{TE}_{PX} \tag{10}$$

Substituting Eqs. (6) and (7) into Eq. (3), and partitioning into F and P type d.o.f., gives

$$\begin{bmatrix}\mathbf{M}_{FF} & \mathbf{M}_{FP}\\ \mathbf{M}_{PF} & \mathbf{M}_{PP}\end{bmatrix}\begin{bmatrix}\mathbf{a}_F^{t+\Delta t}\\ \mathbf{a}_P^{t+\Delta t}\end{bmatrix} + \begin{bmatrix}\mathbf{C}_{FF} & \mathbf{C}_{FP}\\ \mathbf{C}_{PF} & \mathbf{C}_{PP}\end{bmatrix}\left[(1+\alpha)\begin{bmatrix}\dot{\mathbf{a}}_F^{t+\Delta t}\\ \dot{\mathbf{a}}_P^{t+\Delta t}\end{bmatrix} - \alpha\begin{bmatrix}\dot{\mathbf{a}}_F^{t}\\ \dot{\mathbf{a}}_P^{t}\end{bmatrix}\right] + (1+\alpha)\begin{bmatrix}\mathbf{R}_F^{t+\Delta t}\\ \mathbf{R}_P^{t+\Delta t}\end{bmatrix} - \alpha\begin{bmatrix}\mathbf{R}_F^{t}\\ \mathbf{R}_P^{t}\end{bmatrix} = (1+\alpha)\begin{bmatrix}\mathbf{P}_F^{t+\Delta t} + \mathbf{D}_{FX}^{t+\Delta t}\mathbf{X}^{t+\Delta t}\\ \mathbf{P}_P^{t+\Delta t} + \mathbf{D}_{PX}^{t+\Delta t}\mathbf{X}^{t+\Delta t} + \mathbf{S}^{t+\Delta t}\end{bmatrix} - \alpha\begin{bmatrix}\mathbf{P}_F^{t} + \mathbf{D}_{FX}^{t}\mathbf{X}^{t}\\ \mathbf{P}_P^{t} + \mathbf{D}_{PX}^{t}\mathbf{X}^{t} + \mathbf{S}^{t}\end{bmatrix} \tag{11}$$

Transferring the unknowns to the left-hand side leads to

$$\mathbf{M}_{FF}\ddot{\mathbf{a}}_F^{t+\Delta t} + (1+\alpha)\mathbf{C}_{FF}\dot{\mathbf{a}}_F^{t+\Delta t} + (1+\alpha)\mathbf{R}_F^{t+\Delta t} - (1+\alpha)\mathbf{D}_{FX}^{t+\Delta t}\mathbf{X}^{t+\Delta t} = \overline{\mathbf{F}}_F \tag{12}$$

and

$$\begin{aligned}\mathbf{S}^{t+\Delta t} = &-\mathbf{P}_P^{t+\Delta t} - \mathbf{D}_{PX}^{t+\Delta t}\mathbf{X}^{t+\Delta t} + \frac{1}{1+\alpha}\left[\mathbf{M}_{PF}\mathbf{a}_F^{t+\Delta t} + \mathbf{M}_{PP}\mathbf{a}_P^{t+\Delta t}\right]\\ &+ \mathbf{C}_{PF}\dot{\mathbf{a}}_F^{t+\Delta t} + \mathbf{C}_{PP}\dot{\mathbf{a}}_P^{t+\Delta t} + \mathbf{R}_P^{t+\Delta t}\\ &+ \frac{\alpha}{1+\alpha}\left[\mathbf{S}^{t} + \mathbf{P}_P^{t} + \mathbf{D}_{PX}^{t}\mathbf{X}^{t} - \mathbf{C}_{PF}\dot{\mathbf{a}}_F^{t} - \mathbf{C}_{PP}\dot{\mathbf{a}}_P^{t} - \mathbf{R}_P^{t}\right]\end{aligned} \tag{13}$$

where

$$\begin{aligned}\overline{\mathbf{F}}_F = &(1+\alpha)\mathbf{P}_F^{t+\Delta t} - \alpha\mathbf{P}_F^{t} - \alpha\mathbf{D}_{FX}^{t}\mathbf{X}^{t} - \mathbf{M}_{FP}\mathbf{a}_P^{t+\Delta t} - (1+\alpha)\mathbf{C}_{FP}\dot{\mathbf{a}}_P^{t+\Delta t}\\ &+ \alpha\left[\mathbf{C}_{FF}\dot{\mathbf{a}}_F^{t} + \mathbf{C}_{FP}\dot{\mathbf{a}}_P^{t}\right] + \alpha\mathbf{R}_F^{t}\end{aligned} \tag{14}$$

3.2. Incremental formulation for nonlinear analysis

Since the present problem is nonlinear, Eq. (12) is rewritten in the form

$$\boldsymbol{\psi}\left(\mathbf{a}_F^{t+\Delta t}, \mathbf{X}^{t+\Delta t}\right) = \mathbf{0} \tag{15}$$

where $\boldsymbol{\psi}$ is the residual force vector, given by

$$\begin{aligned}\boldsymbol{\psi}\left(\mathbf{a}_F^{t+\Delta t}, \mathbf{X}^{t+\Delta t}\right) = &\overline{\mathbf{F}}_F - \mathbf{M}_{FF}\ddot{\mathbf{a}}_F^{t+\Delta t} - (1+\alpha)\mathbf{C}_{FF}\dot{\mathbf{a}}_F^{t+\Delta t} - (1+\alpha)\mathbf{R}_F^{t+\Delta t}\\ &+ (1+\alpha)\mathbf{D}_{FX}^{t+\Delta t}\mathbf{X}^{t+\Delta t}\end{aligned} \tag{16}$$

The nodal velocities and accelerations depend on the nodal displacements and, for this reason, are not independent unknowns. In the α method the velocity and acceleration at the current time step are approximated with

$$\dot{a}^{t+\Delta t} = \frac{\gamma}{\beta\Delta t}\left(a^{t+\Delta t} - a^{t}\right) + \left(1 - \frac{\gamma}{\beta}\right)\dot{a}^{t} + \Delta t\left(1 - \frac{\gamma}{2\beta}\right)a^{t} \tag{17}$$

$$a^{t+\Delta t} = \frac{1}{\beta\Delta t^2}\left(a^{t+\Delta t} - a^{t}\right) - \frac{1}{\beta\Delta t}\dot{a}^{t} - \left(\frac{1}{2\beta} - 1\right)a^{t} \tag{18}$$

where β and γ are parameters that control the stability and accuracy of the method.

An iterative scheme based on the Newton method [15] is used to solve Eq. (15). Assuming that the solution at the ith iteration has been previously evaluated and neglecting second and higher order terms, the Taylor series for $\boldsymbol{\psi}$ about $\left(\mathbf{a}_F^{t+\Delta t,i}, \mathbf{X}^{t+\Delta t,i}\right)$ is given by

$$\begin{aligned}\boldsymbol{\psi}\left(\mathbf{a}_F^{t+\Delta t,i+1}, \mathbf{X}^{t+\Delta t,i+1}\right) = &\boldsymbol{\psi}\left(\mathbf{a}_F^{t+\Delta t,i}, \mathbf{X}^{t+\Delta t,i}\right)\\ &+ \left[\left.\frac{\partial\boldsymbol{\psi}}{\partial\mathbf{a}_F^{t+\Delta t}}\right|_{\left(\mathbf{a}_F^{t+\Delta t,i}, \mathbf{X}^{t+\Delta t,i}\right)}\right]\left(\mathbf{a}_F^{t+\Delta t,i+1} - \mathbf{a}_F^{t+\Delta t,i}\right)\\ &+ \left[\left.\frac{\partial\boldsymbol{\psi}}{\partial\mathbf{X}^{t+\Delta t}}\right|_{\left(\mathbf{a}_F^{t+\Delta t,i}, \mathbf{X}^{t+\Delta t,i}\right)}\right]\left(\mathbf{X}^{t+\Delta t,i+1} - \mathbf{X}^{t+\Delta t,i}\right)\end{aligned} \tag{19}$$

Substituting Eqs. (16)–(18) into Eq. (19), and assuming that the residual force vector at iteration $i+1$ fulfils the condition given by Eq. (15), leads to

$$\begin{aligned}&\boldsymbol{\psi}\left(\mathbf{a}_F^{t+\Delta t,i}, \mathbf{X}^{t+\Delta t,i}\right)\\ &+ \left[-\frac{1}{\beta\Delta t^2}\mathbf{M}_{FF} - (1+\alpha)\frac{\gamma}{\beta\Delta t}\mathbf{C}_{FF} - (1+\alpha)\left[\left.\frac{\partial\mathbf{R}_F}{\partial\mathbf{a}_F^{t+\Delta t}}\right|_{\mathbf{a}_F^{t+\Delta t,i}}\right]\right]\\ &\times\left(\mathbf{a}_F^{t+\Delta t,i+1} - \mathbf{a}_F^{t+\Delta t,i}\right) + (1+\alpha)\mathbf{D}_{FX}^{t+\Delta t,i}\left(\mathbf{X}^{t+\Delta t,i+1} - \mathbf{X}^{t+\Delta t,i}\right) = 0\end{aligned} \tag{20}$$

Eq. (20) can be rewritten as

$$\overline{\mathbf{K}}_{FF}\Delta\mathbf{a}_F^{i+1} - (1+\alpha)\mathbf{D}_{FX}^{t+\Delta t,i}\Delta\mathbf{X}^{i+1} = \boldsymbol{\psi}\left(\mathbf{a}_F^{t+\Delta t,i}, \mathbf{X}^{t+\Delta t,i}\right) \tag{21}$$

where $\overline{\mathbf{K}}_{FF}$ is the current effective stiffness matrix defined by

$$\overline{\mathbf{K}}_{FF} = \frac{1}{\beta\Delta t^2}\mathbf{M}_{FF} + (1+\alpha)\frac{\gamma}{\beta\Delta t}\mathbf{C}_{FF} + (1+\alpha)\left[\frac{\partial \mathbf{R}_F}{\partial \mathbf{a}_F^{t+\Delta t}}\bigg|_{\mathbf{a}_F^{t+\Delta t,i}}\right] \tag{22}$$

and

$$\Delta\mathbf{a}_F^{i+1} = \mathbf{a}_F^{t+\Delta t,i+1} - \mathbf{a}_F^{t+\Delta t,i} \tag{23}$$

$$\Delta\mathbf{X}^{i+1} = \mathbf{X}^{t+\Delta t,i+1} - \mathbf{X}^{t+\Delta t,i} \tag{24}$$

In matrix notation, Eq. (21) can be expressed as

$$\begin{bmatrix}\overline{\mathbf{K}}_{FF} & \overline{\mathbf{D}}_{FX}\end{bmatrix}\begin{bmatrix}\Delta\mathbf{a}_F^{i+1}\\ \Delta\mathbf{X}^{i+1}\end{bmatrix} = \boldsymbol{\psi}\left(\mathbf{a}_F^{t+\Delta t,i}, \mathbf{X}^{t+\Delta t,i}\right) \tag{25}$$

being

$$\overline{\mathbf{D}}_{FX} = -(1+\alpha)\mathbf{D}_{FX}^{t+\Delta t,i} \tag{26}$$

After the evaluation of the solution at iteration $i+1$, the current residual force vector is calculated using Eq. (16). The iteration scheme continues until the condition

$$\frac{\left|\left|\boldsymbol{\psi}\left(\mathbf{a}_F^{t+\Delta t,i+1}, \mathbf{X}^{t+\Delta t,i+1}\right)\right|\right|}{\left|\left|\mathbf{P}_F^{t+\Delta t}\right|\right|} \leq \varepsilon \tag{27}$$

is fulfilled, being ε a specified tolerance.

4. Contact constraint equations

When contact occurs, the non-penetration condition given by Eq. (2) is fulfilled if

$$\mathbf{v}^{CE} - \mathbf{v}^{TE} = -\mathbf{g} + \mathbf{r} \tag{28}$$

If a contact node is not in contact with any target element, the corresponding constraint equation is not considered.

The displacements of the contact nodes (see Fig. 2) are given by

$$\mathbf{v}^{CE} = \mathbf{H}_{XF}^{CE}\mathbf{a}_F^{t+\Delta t,i+1} + \mathbf{H}_{XP}^{CE}\mathbf{a}_P^{t+\Delta t} \tag{29}$$

where each transformation matrix $\mathbf{H}$ transforms the displacements of the contact nodes from the global coordinate system to the local coordinate system of the contact pair. The displacements of the auxiliary points of the target elements are given by

$$\mathbf{v}^{TE} = \mathbf{H}_{XF}^{TE}\mathbf{a}_F^{t+\Delta t,i+1} + \mathbf{H}_{XP}^{TE}\mathbf{a}_P^{t+\Delta t} \tag{30}$$

where each transformation matrix $\mathbf{H}$ relates the nodal displacements of the target elements, defined in the global coordinate system, with the displacements of the auxiliary points defined in the local coordinate system of each contact pair.

Substituting Eqs. (29) and (30) into Eq. (28) yields

$$\mathbf{H}_{XF}\mathbf{a}_F^{t+\Delta t,i+1} = -\mathbf{g} + \mathbf{r} - \mathbf{H}_{XP}\mathbf{a}_P^{t+\Delta t} \tag{31}$$

where

$$\mathbf{H}_{XF} = \mathbf{H}_{XF}^{CE} - \mathbf{H}_{XF}^{TE} \tag{32}$$

$$\mathbf{H}_{XP} = \mathbf{H}_{XP}^{CE} - \mathbf{H}_{XP}^{TE} \tag{33}$$

Substituting Eq. (23) into Eq. (31) leads to

$$\mathbf{H}_{XF}\Delta\mathbf{a}_F^{i+1} = -\mathbf{g} + \mathbf{r} - \mathbf{H}_{XP}\mathbf{a}_P^{t+\Delta t} - \mathbf{H}_{XF}\mathbf{a}_F^{t+\Delta t,i} \tag{34}$$

Multiplying Eq. (34) by $-(1+\alpha)$ gives

$$\overline{\mathbf{H}}_{XF}\Delta\mathbf{a}_F^{i+1} = \bar{\mathbf{g}} \tag{35}$$

where

$$\overline{\mathbf{H}}_{XF} = -(1+\alpha)\mathbf{H}_{XF} \tag{36}$$

and

$$\bar{\mathbf{g}} = -(1+\alpha)\left(-\mathbf{g} + \mathbf{r} - \mathbf{H}_{XP}\mathbf{a}_P^{t+\Delta t} - \mathbf{H}_{XF}\mathbf{a}_F^{t+\Delta t,i}\right) \tag{37}$$

5. Contact algorithm

The incremental formulation of the equations of motion of the vehicle–structure system, presented in Section 3, is applicable to either linear or nonlinear analyses. These equations and the contact constraints presented in Section 4 form a complete system whose unknowns are incremental nodal displacements and contact forces. Eqs. (25) and (35) can be expressed in matrix form leading to the following system of equations

$$\begin{bmatrix}\mathbf{K}_{FF} & \mathbf{D}_{FX}\\ \overline{\mathbf{H}}_{XF} & \mathbf{0}\end{bmatrix}\begin{bmatrix}\Delta\mathbf{a}_F^{i+1}\\ \Delta\mathbf{X}^{i+1}\end{bmatrix} = \begin{bmatrix}\boldsymbol{\psi}\left(\mathbf{a}_F^{t+\Delta t,i}, \mathbf{X}^{t+\Delta t,i}\right)\\ \bar{\mathbf{g}}\end{bmatrix} \tag{38}$$

Using Betti's theorem, it can be demonstrated that the matrix in Eq. (38) is symmetric. Due to space limitations the corresponding proof is not presented here.

The efficiency of the algorithm used for solving the system of equations is critical. The present methodology uses an efficient and stable block factorization algorithm proposed in [5] that takes into account the specific properties of each block, namely, symmetry, positive definiteness and bandwidth. The Cholesky factorization is also implemented, since for large systems of equations it is generally more efficient than the $\mathbf{LDL}^T$ factorization [16].

A brief summary of the nonlinear dynamic analysis algorithm is presented in Table 1.

6. Numerical example

In order to validate the accuracy and efficiency of the proposed methodology a numerical example consisting of two simply supported spans subjected to four moving sprung masses is presented. The results calculated using the direct method are compared with those obtained with the commercial software ANSYS [14]. In the analysis performed with ANSYS the Lagrange multiplier method is used.

The structure represented in Fig. 3 consists of two simply supported spans modeled with two-dimensional beam elements and subjected to four moving sprung masses (only two are shown). Each span is modeled with 50 finite elements. The geometrical and mechanical properties of the system are the following: length of each span $L = 20$ m, Young's modulus $E = 25$ GPa, Poisson's ratio $\nu = 0.2$, cross-sectional area $A = 6$ m^2, moment of inertia $I = 3$ m^4, mass per unit length $m = 30$ t/m, suspended mass $M_v = 30$ t and spring stiffness $k_v = 156{,}550$ kN/m. The distance between each sprung mass is $d = 20$ m. The fundamental frequency of the simply supported beams is 6.1 Hz and the natural frequency of the spring-mass system is 11.5 Hz.

The sprung masses move at a constant speed $v = 115$ m/s. The time step is $\Delta t = 0.001$ s and the total number of time steps is 900. The vertical accelerations at the midpoint of the first span are plotted in Fig. 4a for $\alpha = 0$, $\beta = 0.25$ and $\gamma = 0.5$, and in Fig. 4b for $\alpha = -0.1$, $\beta = 0.3025$ and $\gamma = 0.6$.

A nonzero value of the α parameter is useful for controlling the spurious participation of the higher modes shown in Fig. 4a. Hence, the analyses presented in the remainder of this section are performed using $\alpha = -0.1$.

The vertical displacements and accelerations at the midpoint of the first span, obtained with both the direct method and ANSYS, are plotted in Figs. 5 and 6. The vertical displacements of the first and fourth sprung masses are compared in Fig. 7. The results obtained with the direct method and ANSYS show an excellent

Table 1
Summary of the nonlinear dynamic analysis algorithm.

1. Factorize $\overline{\mathbf{K}}_{FF}$ and calculate $\mathbf{L}_{21}$ (see [5])
2. Start the time integration loop ($t = 0$)
3. Calculate the external load vector $\mathbf{P}^{t+\Delta t}$
4. Assume the following predictors for the accelerations and contact forces:
   (a) $\mathbf{a}_F^{t+\Delta t} = \mathbf{0}$
   (b) $\mathbf{X}^{t+\Delta t} = \mathbf{X}^t$
   Calculate the initial displacements and velocities:
   (a) $\mathbf{a}_F^{t+\Delta t} = \mathbf{a}_F^t + \dot{\mathbf{a}}_F^t \Delta t + (1/2 - \beta)\mathbf{a}_F^t \Delta t^2$
   (b) $\dot{\mathbf{a}}_F^{t+\Delta t} = \dot{\mathbf{a}}_F^t + (1 - \gamma)\mathbf{a}_F^t \Delta t$
5. Start the Newton iteration loop ($i = 0$)
6. Check the contact status using Eq. (2) and calculate matrices **D** and **H** for the existing constraints
7. Evaluate the residual force vector $\boldsymbol{\psi}(\mathbf{a}_F^{t+\Delta t,i}, \mathbf{X}^{t+\Delta t,i})$ using Eq. (16)
8. Check the convergence criteria (ε is a specified tolerance):
   (a) if $\|\boldsymbol{\psi}\|/\|\mathbf{P}_F^{t+\Delta t}\| \leqslant \varepsilon$, convergence achieved; continue to next time step (step 3)
   (b) if $\|\boldsymbol{\psi}\|/\|\mathbf{P}_F^{t+\Delta t}\| > \varepsilon$, convergence not achieved; continue to step 9
9. If required, update the effective stiffness matrix using Eq. (22)
10. Solve the system of Eq. (38) using the block factorization solver (see [5]) to obtain $\Delta\mathbf{a}_F^{i+1}$ and $\Delta\mathbf{X}^{i+1}$
11. Update the displacements, velocities, accelerations and contact forces:
    (a) $\mathbf{a}_F^{t+\Delta t,i+1} = \mathbf{a}_F^{t+\Delta t,i} + \Delta\mathbf{a}_F^{i+1}$
    (b) $\dot{\mathbf{a}}_F^{t+\Delta t,i+1} = \frac{\gamma}{\beta\Delta t}\left(\mathbf{a}_F^{t+\Delta t,i+1} - \mathbf{a}_F^t\right) + \left(1 - \frac{\gamma}{\beta}\right)\dot{\mathbf{a}}_F^t + \Delta t\left(1 - \frac{\gamma}{2\beta}\right)\mathbf{a}_F^t$
    (c) $\mathbf{a}_F^{t+\Delta t,i+1} = \frac{1}{\beta\Delta t^2}\left(\mathbf{a}_F^{t+\Delta t,i+1} - \mathbf{a}_F^t\right) - \frac{1}{\beta\Delta t}\dot{\mathbf{a}}_F^t - \left(\frac{1}{2\beta} - 1\right)\mathbf{a}_F^t$
    (d) $\mathbf{X}^{t+\Delta t,i+1} = \mathbf{X}^{t+\Delta t,i} + \Delta\mathbf{X}^{i+1}$
12. Increment the iteration counter i and continue to step 6

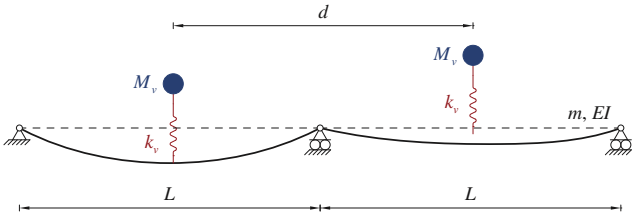

Fig. 3. Two simply supported spans subjected to a set of moving sprung masses.

agreement. The slight differences observed in Fig. 6 may be due to the fact that the contact elements available in ANSYS use linear displacement interpolation functions and the contact elements presented in this paper use cubic functions.

Finally, the contact forces of the first and fourth sprung masses are plotted in Fig. 8. The results obtained with the direct method perfectly match the corresponding ANSYS solutions obtained using the classical Lagrange multiplier method. The first sprung mass is in contact with the beam during the analysis period, since the motion of the beam is not large enough to cause a separation. However, as can be observed in Fig. 8b), a null contact force in the fourth sprung mass indicates the occurrence of a separation. Therefore, it can be concluded that the proposed methodology is capable of accurately modeling the contact and separation between two bodies.

In order to assess the computational efficiency of the algorithm the two simply supported spans are now modeled with 16,000 eight-node solid elements ($2 \times 80 \times 10 \times 10$), as shown in Fig. 9. This model has 58,696 unconstrained d.o.f. and a square cross section of width $b = 2.45$ m, in correspondence with the geometrical properties of the previous beams.

The vertical displacement at the midpoint of the first span is plotted in Fig. 10, while the vertical displacement of the fourth sprung mass is shown in Fig. 11. The contact force of the fourth

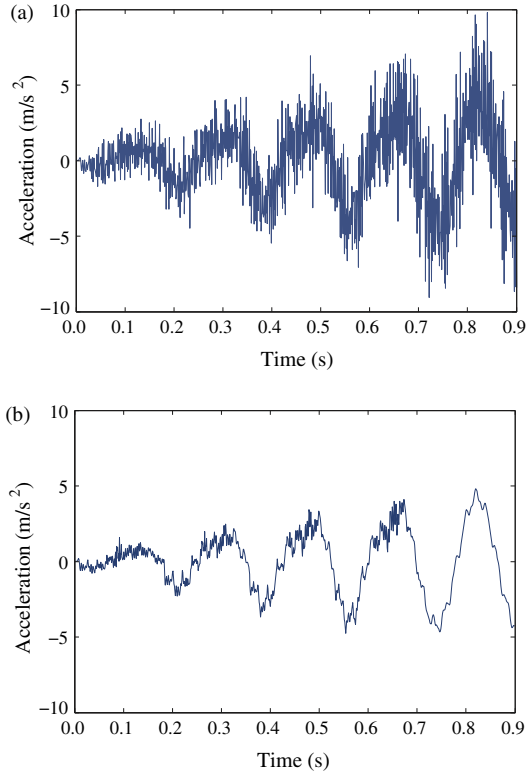

Fig. 4. Vertical acceleration at the midpoint of the first span considering (a) $\alpha = 0$ and (b) $\alpha = -0.1$.

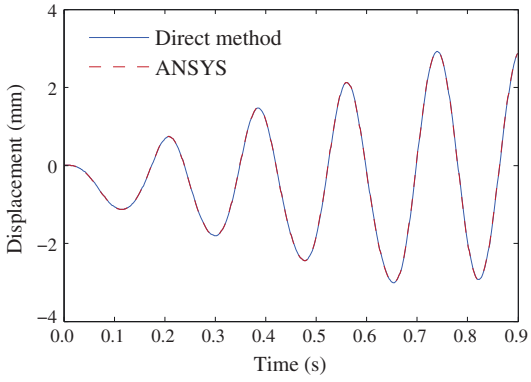

Fig. 5. Vertical displacement at the midpoint of the first span.

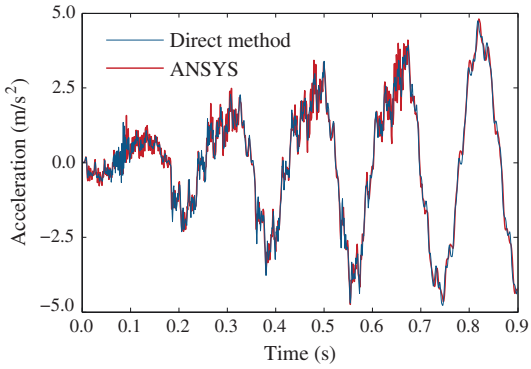

Fig. 6. Vertical acceleration at the midpoint of the first span.

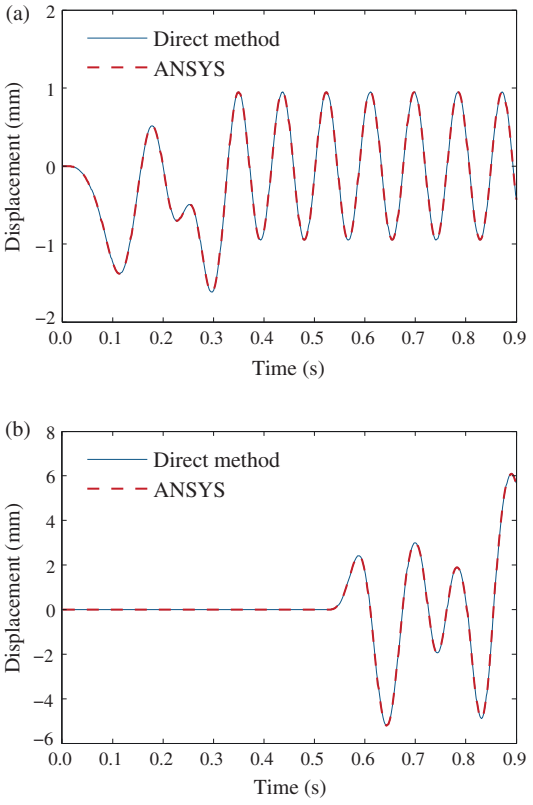

Fig. 7. Vertical displacement of the (a) first and (b) fourth sprung masses.

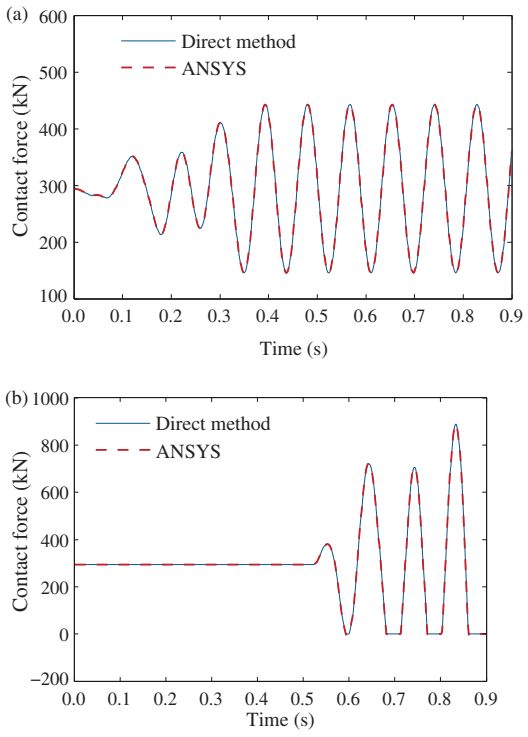

Fig. 8. Normal contact force of the (a) first and (b) fourth sprung masses.

sprung mass is depicted in Fig. 12. Once more the results obtained with the proposed methodology show a good agreement with the corresponding ANSYS solutions.

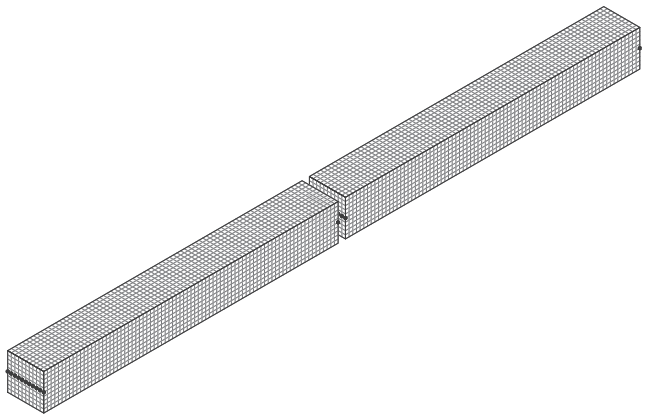

Fig. 9. Two simply supported spans modeled with 3D solid elements.

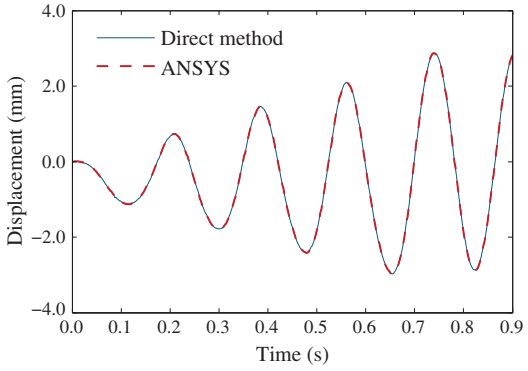

Fig. 10. Vertical displacement at the midpoint of the first span.

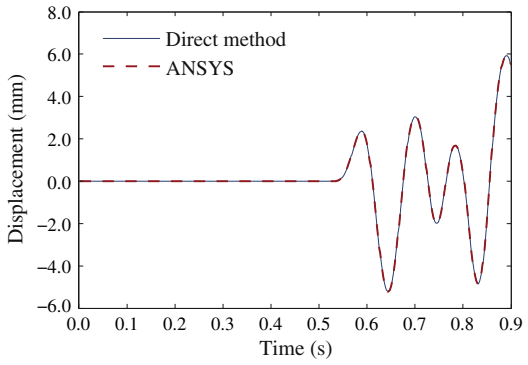

Fig. 11. Vertical displacement of the fourth sprung mass.

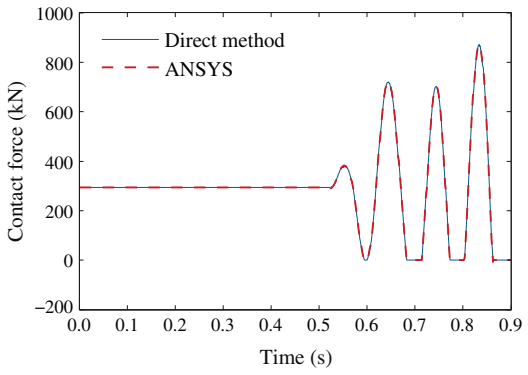

Fig. 12. Normal contact force of the fourth sprung mass.

All the calculations have been performed using a workstation with an Intel Xeon E5620 dual core processor running at 2.40 GHz. For a more accurate comparison, the calculations in ANSYS and MATLAB have been performed using a single execution thread. In the 900 time steps, a total of 1026 iterations have been performed with a maximum of 2 iterations in the time steps that require a change in the contact status. A convergence tolerance of $\varepsilon = 10^{-6}$ is used (see Section 3.2). The elapsed time is 16,623 s using ANSYS and 261 s using the direct method with the optimized block factorization algorithm, which is about 64 times faster.

7. Conclusions

An accurate, efficient and robust method for analyzing the nonlinear vehicle–structure interaction is presented. The direct method is used to formulate the governing equilibrium equations and impose the constraint equations that relate the displacements of the contact node with the displacements of the corresponding target element. The accuracy of the method has been confirmed using a numerical example, in which the results obtained with the direct method and ANSYS show an excellent agreement.

The proposed method uses an optimized block factorization algorithm to solve the system of linear equations. The performed numerical analyses demonstrate the efficiency of the developed algorithm, since the calculations performed using the direct method are 64 times faster than the calculations performed with ANSYS.

Since in the present method the tangential creep forces acting at the interface are not considered, the lateral vehicle–structure interaction cannot be taken into account. To determine these forces, the material and geometric properties of the wheel and rail, and also the relative velocity between the two bodies at the contact point have to be considered. The extension of the present method to three-dimensional contact problems is under development and will be presented in a forthcoming publication.

Acknowledgements

The authors wish to thank Professor Rui Faria of the University of Porto for the helpful discussions during the preparation of this manuscript, especially regarding the incremental formulation used in this work. This article reports research developed under financial support provided by "FCT - Fundação para a Ciência e Tecnologia", Portugal, under Grants SFRH/BD/39190/2007 and SFRH/BD/48320/2008.

References

[1] Pombo J, Ambrosio J, Silva M. A new wheel–rail contact model for railway dynamics. Veh Syst Dynam 2007;45:165–89. http://dx.doi.org/10.1080/00423110600996017.
[2] Shabana A, Zaazaa KE, Escalona JL, Sany JR. Development of elastic force model for wheel/rail contact problems. J Sound Vib 2004;269:295–325. http://dx.doi.org/10.1016/S0022-460X(03)00074-9.
[3] Antolín P, Goicolea JM, Oliva J, Astiz MA. Nonlinear train–bridge lateral interaction using a simplified wheel–rail contact method within a finite element framework. J Comput Nonlinear Dynam 2012;7. http://dx.doi.org/10.1115/1.400673. Art. no. 041014.
[4] Tanabe M, Matsumoto N, Wakui H, Sogabe M, Okuda H, Tanabe Y. A simple and efficient numerical method for dynamic interaction analysis of a high-speed train and railway structure during an earthquake. J Comput Nonlinear Dynam 2008;3. http://dx.doi.org/10.1115/1.296048. Art. no. 041002.
[5] Neves SGM, Azevedo AFM, Calçada R. A direct method for analyzing the vertical vehicle–structure interaction. Eng Struct 2012;34:414–20. http://dx.doi.org/10.1016/j.engstruct.2011.10.010.
[6] Yang YB, Wu YS. A versatile element for analyzing vehicle–bridge interaction response. Eng Struct 2001;23:452–69. http://dx.doi.org/10.1016/S0141-0296(00)00065-1.
[7] Wriggers P. Computational contact mechanics. Chichester, UK: John Wiley & Sons Ltd.; 2002.
[8] Delgado R, Santos SM. Modelling of railway bridge–vehicle interaction on high speed tracks. Comput Struct 1997;63:511–23. http://dx.doi.org/10.1016/S0045-7949(96)00360-4.
[9] Lei X, Noda NA. Analyses of dynamic response of vehicle and track coupling system with random irregularity of track vertical profile. J Sound Vib 2002;258:147–65. http://dx.doi.org/10.1006/jsvi.2002.5107.
[10] Nguyen D-V, Kim K-D, Warnitchai P. Dynamic analysis of three-dimensional bridge-high-speed train interactions using a wheel–rail contact model. Eng Struct 2009;31:3090–106. http://dx.doi.org/10.1016/j.engstruct.2009.08.015.
[11] Yang F, Fonder G. An iterative solution method for dynamic response of bridge–vehicles systems. Earthquake Eng Struct Dynam 1996;25:195–215. http://dx.doi.org/10.1002/(SICI)1096-9845(199602)25:2<195::AID-EQE547>3.0.CO;2-R.
[12] Hilber HM, Hughes TJR, Taylor RL. Improved numerical dissipation for time integration algorithms in structural dynamics. Earthquake Eng Struct Dynam 1977;5:283–92. http://dx.doi.org/10.1002/eqe.4290050306.
[13] MATLAB®. R2011b. The MathWorks Inc., Natick, MA; 2011.
[14] ANSYS®. Academic research. Release 13.0. ANSYS Inc., Canonsburg, PA; 2010.
[15] Owen DRJ, Hinton E. Finite elements in plasticity: theory and practice. Swansea, UK: Pineridge Press Limited; 1980.
[16] Burden RL, Faires JD. Numerical analysis. 6th ed. Pacific Grove, CA: ITP; 1997.